



Mining-related ground deformation in Crescent Valley, Nevada: Implications for sparse GPS networks

Noel Gourmelen,¹ Falk Amelung,¹ Francesco Casu,² Mariarosaria Manzo,² and Riccardo Lanari²

Received 21 January 2007; revised 9 March 2007; accepted 10 April 2007; published 8 May 2007.

[1] We use the Small Baseline Subset (SBAS) InSAR algorithm to obtain radar line-of-sight deformation velocities for two adjacent SAR swaths and invert the data for the 2-D velocity field in vertical and ground range direction. The analysis reveals areas of rapid deformation caused by mining and agricultural activities in the Crescent Valley, Nevada, USA. The LOS displacements of up to 25 centimeters during the 1992–2002 period are caused by vertical and horizontal deformation. About 8 mm/yr horizontal velocity is detected 10 km from the BARGEN GPS site LEWI suggesting that the GPS station may be moving in response to the water pumping. In the Basin and Range anthropogenic ground deformation can extend several tens of kilometers from the basins into the bedrock of the Ranges. **Citation:** Gourmelen, N., F. Amelung, F. Casu, M. Manzo, and R. Lanari (2007), Mining-related ground deformation in Crescent Valley, Nevada: Implications for sparse GPS networks, *Geophys. Res. Lett.*, *34*, L09309, doi:10.1029/2007GL029427.

1. Introduction

[2] Global Positioning System measurements over the last 15 years have provided new insights into the contemporaneous deformation of the Basin and Range Province in the western USA [Thatcher *et al.*, 1999; Wernicke *et al.*, 2000; Hammond and Thatcher, 2005]. The dominant deformation modes are right-lateral shear and extension along the western and eastern margins (in zones referred to as the Walker Lane and Central Nevada Seismic Belt, CNSB, and Wasatch fault) [Dixon *et al.*, 1995; Malservisi *et al.*, 2003], whereas the Central Basin and Range behaves as a stable block [Bennett *et al.*, 2003; Gourmelen and Amelung, 2005]. However, the motions of some GPS stations of the Basin and Range Geodetic Network (BARGEN) deviate from this simple deformation field [Wernicke *et al.*, 2000; Friedrich *et al.*, 2003; Hammond and Thatcher, 2005]. The most prominent example is the GPS station LEWI on the Mt Lewis in the Shoshone mountain range west of the Crescent Valley (Figure 1). LEWI moves 2–3 mm/yr southeast with respect to the neighboring stations (Figure 1a) [Wernicke *et al.*, 2000; Bennett *et al.*, 2003; Friedrich *et al.*, 2004]. This is best illustrated by plotting its velocity in a reference frame

fixed to the stations NEWS and MINE (blue arrows in Figure 1a, red arrows are velocities from Bennett *et al.* [2003] with respect to stable North America). LEWI's motion corresponds to crustal shortening of the Crescent Valley area, which is not consistent with the overall extension in the region [Friedrich *et al.*, 2004]. Although mining is occurring in the Crescent Valley possible interaction has been considered unlikely because of the distance from LEWI to the mine and because mining-induced deformation is occurring in the sediment fill. Gourmelen and Amelung [2005] used Interferometric Synthetic Aperture Radar (InSAR) to find evidence of transient deformation following a series of 1915–54 earthquakes in Western Nevada but their model does not explain the motion of LEWI. We exploit multi-temporal InSAR interferograms and generate radar LOS displacement time series and velocity maps for two adjacent SAR swaths. We invert the data in the overlapping region to retrieve the ground velocity components in the vertical and ground range direction. We show that the mining activities can produce significant horizontal deformation likely to account for part of the movement of GPS even in bedrock environment.

2. InSAR Data

[3] We used ERS1,2 SAR data, frame 2799, tracks 442 and 170. The satellite tracks (descending with the satellite traveling south) are adjacent resulting in a 30 km overlap of the imaged area at this latitude (Figure 1a). InSAR measures ground displacements in the radar line-of-sight direction (LOS). The look angle varies across a full ERS SAR image from about 19° in the near range to 27° in the far range. The images overlap by more than one third of the image width so that for the Crescent Valley there is a difference in the LOS direction of 4.0° (Figures 1a and 2c).

[4] We processed the SAR data into LOS velocity maps using the Small Baseline Subset (SBAS) methodology [Berardino *et al.*, 2002; Lanari *et al.*, 2004; Casu *et al.*, 2006]. In the SBAS method, multiple interferograms with small baselines are pixel-wise inverted for the phase history with respect to the first acquisition. After conversion into a LOS displacement time series a time-averaged velocity is estimated. For each SAR acquisition we use the 5 interferograms with the smallest perpendicular baseline as long as it is less than 400 m and the temporal separation is less than 4 years. A temporal and spatial filtering removes linear phase contributions that are correlated in space but not in time such as related to errors in the satellite orbits. For this, the phase history for each pixel is smoothed using a triangular filter with a filter length of about 2 years. For each acquisition, the difference between the smoothed and

¹Rosenstiel School of Marine and Atmospheric Science, Division of Marine Geology and Geophysics, University of Miami, Miami, Florida, USA.

²Istituto per il Rilevamento, Elettromagnetico dell'Ambiente, Consiglio Nazionale delle Ricerche, Naples, Italy.

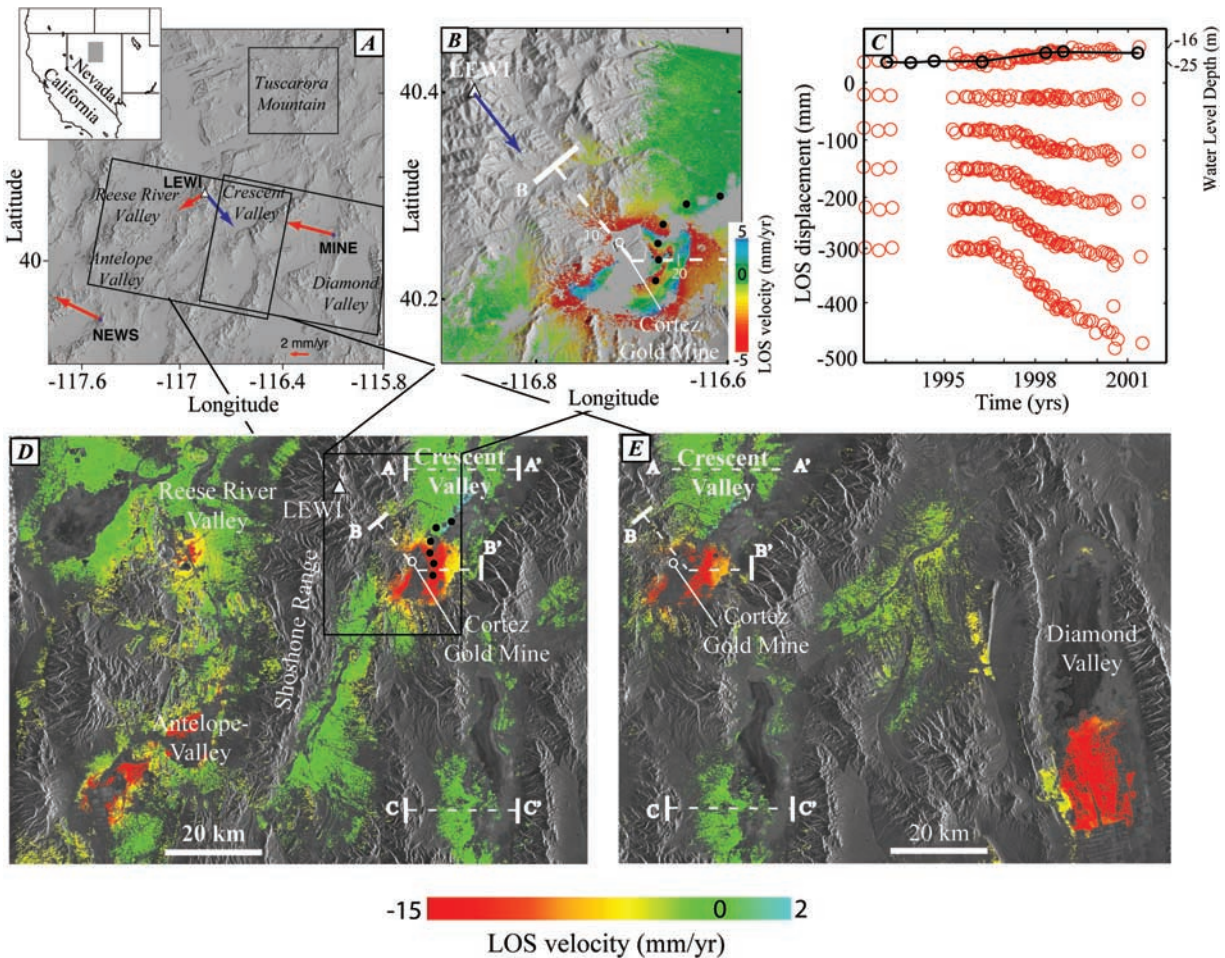


Figure 1. InSAR deformation velocity maps. (a) Shaded relief of the study area and permanent GPS stations from the BARGEN network. GPS motion is with respect to stable North America (red arrows) and with respect to nearby GPS stations NEWS and MINE (blue arrow). Black boxes: location of InSAR derived rate maps. (b) Rate velocity map over Crescent Valley (subset of Figure 1d). GPS station LEWI and residual velocity (blue arrow). Location of profile on Figure 2 (white dashed line) and distance marks. Color scale wrapped for better visibility. (c) Time series of deformation from 1992 to 2002, from (top) away to (bottom) within the Crescent valley subsidence area. Black circles are water level at a well collocated with the top time series showing linear relationship between surface deformation and water level. (d, e) Rate velocity maps of the subsidence at Crescent Valley, Diamond valley, Reese River Valley and Antelope Valley. Maps obtained from processing of two adjacent radar tracks (track 442 and track 170). White lettering: location of profile of Figure 2. Black dots: location of time series of deformation (Figure 1d) arranged in the order of time series (Figure 1c). The color scale is saturated at -15 mm/yr.

the original phase is then approximated by a linear phase ramp simulating the orbit error for this acquisition. Modified interferograms are formed by removing the estimated orbital phase ramps, the displacement histories and averaged velocities are then recalculated. We finally remove linear ramps from the LOS velocity fields related to residual orbital errors after filtering [Casu *et al.*, 2006; Bürgmann *et al.*, 2006].

[5] The LOS velocity maps show 4 areas of LOS increase of up to several centimeters per year in the Crescent Valley (Figures 1b, 1d, and 1e), Antelope Valley (Figure 1d), Reese River Valley (Figure 1d) and Diamond Valley (Figure 1e). These areas are mining and agricultural fields, suggesting that we see anthropogenic ground movements.

[6] In the Crescent Valley, the maximum LOS increase occurs 4 km east of the open-pit Cortez mine. The time

histories of LOS displacement with respect to the first acquisition along a cross-section through Crescent Valley indicate up to 250 mm of displacement between 1996 and 2002 in the center of the deforming area, corresponding to a LOS velocity of 40 mm/yr (lower time series in Figure 1c). Subtle uplift of 12 mm (2 mm/yr) is detected 20 km northeast of the mine (top time series in Figure 1c), likely associated with the surface discharge of groundwater pumped from the bottom of the open pit. LOS increase started in summer 1996 (Figure 1c), when the exploitation of the mine began. The rate of LOS increase was nearly linear until the end of 1998. Then, the ground velocities diminished, in particular at the edge of the deforming system as well as within the area of uplift. For simplicity, we approximate the deformation by a linear velocity for the 1996–2002 period.

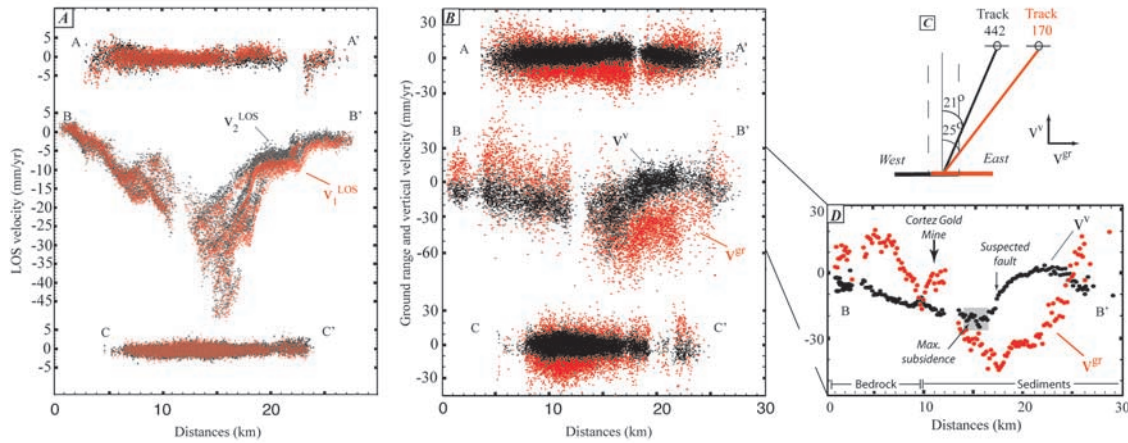


Figure 2. Vertical and ground range velocity inversion (see location of profiles in Figures 1d and 1e). (a) East-west profiles across track 442 derived deformation rate map (v_2^{LOS} , black) and track 170 derived deformation rate map (v_1^{LOS} , red). (5 km Profiles width). For better visualization of the difference, the data for track 170 (v_1^{LOS}) have been shifted downwards by 3 mm/yr with respect to the data for track 442 (v_2^{LOS}) on profile B-B'. (b) Inversion for ground range and vertical velocities for the three profiles in Figure 2a. The B-B' profiles shows ground range and vertical deformation whereas A-A' and C-C' do not. The scatter of the points appears higher when point density is higher but is in fact similar. (c) Sketch showing the principle of the inversion based on overlapping area and angle difference of two adjacent radar tracks. (d) Filtered profile B-B' from Figure 2b. Areas of surface bedrock and sediments is indicated.

[7] The ground displacements are roughly consistent with water level measurements. No data are available for the subsiding area but well data in the uplift area in the north show a significant water level rise between 1996 and 1998 and then a stabilization of the water level (black circles and line in Figure 1c).

[8] A profile through the deforming area of the Crescent Valley shows a subtle difference in LOS velocity of up to 3 mm/yr between the two swaths (at 15–25 km distance along profile B-B', Figure 2a). No similar difference occurs in the non-deforming areas further north and south (profiles A-A' and C-C', Figure 2a), suggesting that it is related to the difference in radar incidence angle on the ground (Figure 2c).

3. The 2-D Ground Velocity Field From Overlapping Satellite Swaths

[9] The horizontal component of the velocity vector in LOS direction (the ground range velocity), v^{gr} , and the vertical component, v^v , (Figure 2c) are related to the measured LOS velocities, $v_{1,2}^{LOS}$, by

$$\begin{pmatrix} v_1^{LOS} \\ v_2^{LOS} \end{pmatrix} = \begin{pmatrix} \sin(\theta_1) \cos(\theta_1) \\ \sin(\theta_2) \cos(\theta_2) \end{pmatrix} \cdot \begin{pmatrix} v^{gr} \\ v^v \end{pmatrix} \quad (1)$$

with $\theta_{1,2}$ the radar incidence angles for the two interferograms (see Wright *et al.* [2004] for a more general formulation). From this we obtain:

$$v^{gr} = \frac{v_1^{LOS} - v_2^{LOS} \cdot \frac{\cos \theta_1}{\cos \theta_2}}{\sin \theta_1 - \sin \theta_2 \cdot \frac{\cos \theta_1}{\cos \theta_2}} \quad (2)$$

$$v^v = \frac{v_1^{LOS} - v_2^{LOS} \cdot \frac{\sin \theta_1}{\sin \theta_2}}{\cos \theta_1 - \cos \theta_2 \cdot \frac{\sin \theta_1}{\sin \theta_2}} \quad (3)$$

[10] The v^{gr} and v^v for the 3 profiles are shown in Figure 2b and averaged curves for the B-B' profile is shown in Figure 2d. For the deforming area, v^v varies from -6 mm/yr at the beginning of the profile to a maximum of -20 mm/yr at 16–17 km distance and is slightly positive ($+1.5$ mm/yr) at 18–21 km distance (Figure 2d). The latter could be the result of local faulting, uplift similar to the uplifting bulge in the perimeter region of surface loads, or is introduced by a systematic error discussed below. The pattern of the horizontal velocity v^{gr} is consistent with the expected convergent motion towards a pumping source as reflected by a positive v^{gr} west of, and a negative v^{gr} east of the deforming center. However, v^{gr} is asymmetric. The amplitude of v^{gr} is higher in the east than in the west (Figure 2d) and the null horizontal velocity point is offset westward with respect to the maximum vertical velocity point. This contrast with the symmetric deformation field expected from Biot's theory of poro-elasticity. This difference possibly reveals the laterally varying thickness of the basin fill, thicker in the east where the basin is bounded by a west-dipping normal fault. Underlying bedrock may account for some of the deformation within the basin or faults may act as barriers for ground water flow [Amelung *et al.*, 1999].

[11] Along the profile to the south, v^{gr} and v^v are approximately zero as expected for a non-deforming area (Figure 2b, profile C-C'). Along the profile to the north v^{gr} is zero but v^v is slightly positive (Figure 2b, profile A-A') due to the subtle uplift associated with the release of the pumped water noted in Figure 1c.

4. Measurement Uncertainties of the InSAR Data

[12] The uncertainties associated with measurements of the LOS displacements u^{LOS} depends on how well atmospheric, topographic, and orbital contributions have been corrected by the SBAS processing algorithm, and on the distance of a pixel to the reference point. We find for the

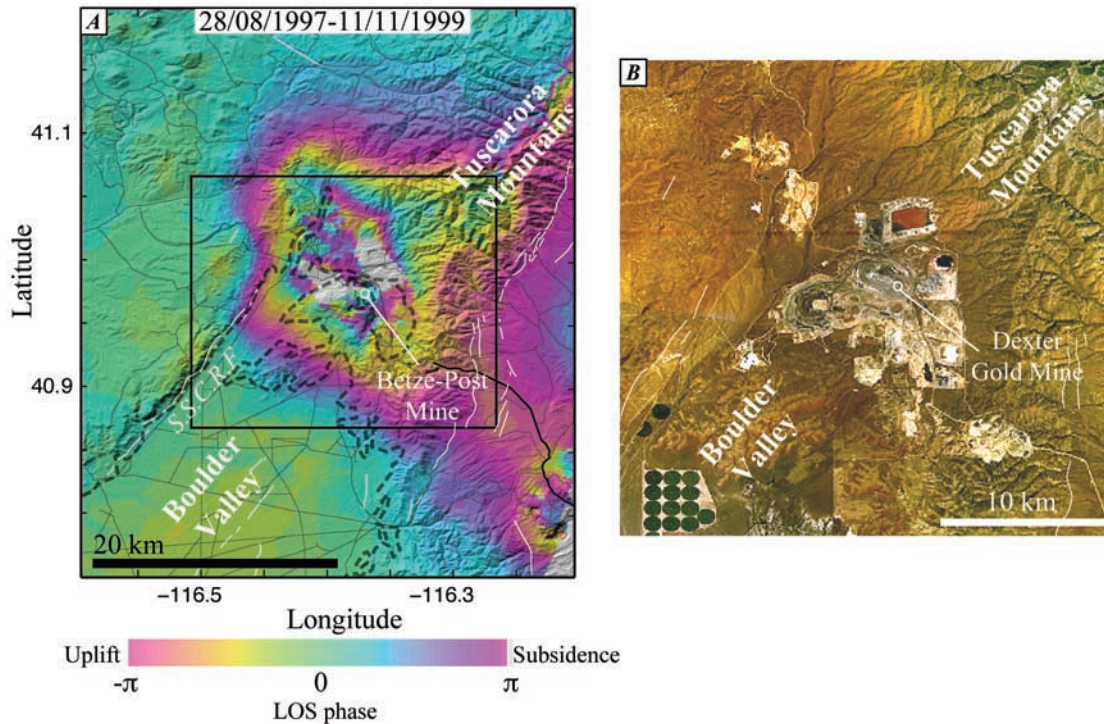


Figure 3. Bedrock subsidence (a) 2 years interferogram of the bedrock subsidence in Tuscarora mountain over shaded relief of topography. Southern Sheep Creek Range Fault (S.S.C.R.F.). Faults (white lines), main roads (grey lines), bedrock-sediment limit (dashed black line). (b) Landsat image of the Dexter Mine complex.

vicinity of the reference point in a non-deforming area a standard deviation of $\sigma_{u^{LOS}} = 2$ mm. The spatial gradient of the standard deviation is 0.05 mm per kilometer from the reference point.

[13] The velocity estimates v^{LOS} , v^{gr} , v^v uncertainty is a complex function of the uncertainty of the u^{LOS} measurements and their correlation, on the temporal spacing of the SAR acquisitions and on the time period covered. For a sample of 10000 pixels in a 15 km non-deforming area, we find a standard deviations of $\sigma_{v^{LOS}} = 0.6$ mm/yr, $\sigma_{v^{gr}} = 9$ mm/yr and $\sigma_{v^v} = 4$ mm/yr and a negligible dependence on the distance to the reference point. The distributions for v^{LOS} are slightly asymmetric narrower than a Gaussian distribution with 85% and 97% of the samples within the 1σ and the 2σ intervals respectively. The distributions for v^{gr} and v^v on the other hand are well approximated by a Gaussian distribution with 69% and 95% of the samples within the 1σ and 2σ intervals, indicating that the standard deviations are acceptable uncertainty measures. They are 10% smaller than the expected values from linear error propagation of equations (2) and (3).

5. Ground Velocity at GPS Station LEWI

[14] The GPS station LEWI is located 22 km to the northwest of the center of the Crescent Valley deforming area at 18 km from the Cortez mine (Figure 1b). LEWI moves 2–3 mm/yr southeast with respect to the neighboring stations. This corresponds to 1.5–2.5 mm/yr in ground range direction (the angle between LEWI's velocity and the ground range direction is $\sim 35^\circ$). No InSAR measure-

ments are available from the SBAS analysis for LEWI for direct comparison with the GPS data because it is located in frequently snow-covered mountains.

[15] About 9 km from LEWI at the start of the profile B-B' we have inferred a velocity of $8 + -9$ mm/yr in ground range direction (Figures 2b and 2d) Although we do not know how rapidly the deformation decays with distance from the pumping sites it seems very plausible that LEWI's apparently anomalous motion is caused by the Crescent Valley pumping activities. This is consistent with the observation that LEWI moves towards the center of the deforming area.

6. Bedrock Deformation in Response to Water Level Changes

[16] We have shown that ground water pumping is causing horizontal and vertical ground deformation in bedrock at a distance of several tens of km to the pumping site. This is in contrast to previous observations, for example in the Los Angeles basin [Bawden *et al.*, 2001] and Las Vegas valley [Amelung *et al.*, 1999; Bell *et al.*, 2002]. Deformation is attributed to sediment compaction with both vertical and horizontal displacement [Watson *et al.*, 2002; Argus *et al.*, 2005]. Recently, Burbey *et al.* [2005] showed that pumping can be associated with horizontal deformation of the same magnitude as the vertical deformation.

[17] A spectacular example for pumping-induced bedrock deformation occurs in the Tuscarora Mountains (Figure 3) 50 km northeast of the Cortez mine. The total LOS

displacement through the 1992–2001 period reaches 30 cm. The deformation follows the mapped faults at the eastern margin of the Tuscarora mountains. The small valleys south of the mine have no effect on the deformation pattern suggesting a relatively deep source for the deformation (deeper than the valley fills) [Katzenstein and Bell, 2006].

[18] Possible mechanisms for the large-scale pumping-induced bedrock deformation are poro-elastic deformation and the contraction or expansion of the rock mass by closing and opening of fractures and fault gouge in response to water level changes [Cappa et al., 2006]. We would expect horizontal deformation perpendicular to the strike direction. This is consistent with deformation pattern in the eastern Tuscarora mountains where the displacement gradient is perpendicular to the faults and consistent with LEWI's motion perpendicular to the Shoshone Range's strike. Another explanation would be that the bedrock composition of both the Shoshone Range (LEWI's bedrock) and the Tuscarora Mountain contains shale and argillite, two rock type rich in clay, a mineral whose volume is very dependant of water content.

7. Conclusions

[19] We have applied the SBAS-InSAR technique in order to estimate LOS mean deformation velocity maps for two adjacent SAR swaths. The presented analysis reveals a distinct deforming area, located in the Crescent Valley, Nevada, with LOS velocities of up to 40 mm/yr caused by ground water pumping in support of mining activities. Inversion of the InSAR data for the 2-D velocity field, in the overlapping SAR swaths region, indicates subsidence and convergent horizontal deformation. Pumping-induced ground deformation may explain the enigmatic motion of the GPS station LEWI. Pumping-induced ground deformation can occur in bedrock at a distance larger than 20 km from the pumping site and needs to be evaluated prior to the geodynamic interpretation of sparse GPS velocity field.

[20] **Acknowledgments.** We thank J. Bell for useful comments on an early version of the manuscript and Gerald W. Bawden and an anonymous reviewer for a detailed review that help improve the paper. The Division of Water Resources of the state of Nevada provided the Well data. The InSAR data were provided by the European Space Agency (ESA) through a category 1 project and by the Western North America Interferometric Synthetic Aperture Radar Consortium (WinSAR). Funding was provided by NASA's Solid Earth and Natural Hazard program and the NSF Earthscope program. CSTARS contribution # 14. N.G. is supported by the NASA Earth System Science fellowship.

References

- Amelung, F., D. L. Galloway, J. W. Bell, H. A. Zebker, and R. J. Lacznik (1999), Sensing the ups and down of Las Vegas—InSAR reveals structural control of land subsidence and aquifer-system deformation, *Geology*, *27*, 483–486.
- Argus, D. F., M. B. Heflin, G. Peltzer, F. Crampé, and F. H. Webb (2005), Interseismic strain accumulation and anthropogenic motion in metropolitan Los Angeles, *J. Geophys. Res.*, *110*, B04401, doi:10.1029/2003JB002934.
- Bawden, G. W., W. Thatcher, R. S. Stein, K. W. Hudnut, and G. Peltzer (2001), Tectonic contraction across Los Angeles after removal of ground-water pumping effects, *Nature*, *412*, 812–815.
- Bell, J., F. Amelung, A. R. Ramelli, and G. Blewitt (2002), Land subsidence in Las Vegas, Nevada, 1935–2000: New geodetic data show evolution, revised spatial patterns, and reduced rates, *Environ. Eng. Geosci.*, *8*(3), 155–174.
- Bennett, R. A., B. P. Wernicke, N. A. Niemi, A. M. Friedrich, and J. L. Davis (2003), Contemporary strain rates in the northern Basin and Range province from GPS data, *Tectonics*, *22*(2), 1008, doi:10.1029/2001TC001355.
- Berardino, P., G. Fornaro, R. Lanari, and E. Sansosti (2002), A new algorithm for surface deformation monitoring based on small baseline differential SAR interferograms, *IEEE Trans. Geosci. Remote Sens.*, *40*, 2375–2383.
- Burbey, T. J., S. M. Warner, G. Blewitt, J. W. Bell, and E. Hill (2005), Three-dimensional deformation and strain induced by municipal pumping, part 1: Analysis of field data, *J. Hydrol.*, *319*, 123–142, doi:10.1016/j.jhydrol.2005.06.028.
- Bürgmann, R., G. Hilley, A. Ferretti, and F. Novali (2006), Resolving vertical tectonics in the San Francisco Bay area from GPS and permanent scatterer InSAR analysis, *Geology*, *34*, 221–224.
- Cappa, F., Y. Guglielmi, S. Gaffet, H. Lancon, and I. Lamarque (2006), Use of in situ fiber optic sensors to characterize highly heterogeneous elastic displacement fields in fractured rocks, *Int. J. Rock Mech. Min. Sci.*, *43*, 647–654.
- Casu, F., M. Manzo, and R. Lanari (2006), A quantitative assessment of the SBAS algorithm performance for surface deformation retrieval from DInSAR data, *Remote Sens. Environ.*, *102*, 95–210, doi:10.1016/j.rse.2006.01.023.
- Dixon, T. H., S. Robaudo, J. Lee, and Reheis (1995), Constraints on present day basin and range deformation from space geodesy, *Tectonics*, *14*, 755–772.
- Friedrich, A. M., B. P. Wernicke, N. A. Niemi, R. A. Bennett, and J. L. Davis (2003), Comparison of geodetic and geologic data from the Wasatch region, Utah, and implications for the spectral character of Earth deformation at periods of 10 to 10 million years, *J. Geophys. Res.*, *108*(B4), 2199, doi:10.1029/2001JB000682.
- Friedrich, A. M., J. Lee, B. P. Wernicke, and K. Sieh (2004), Geologic context of geodetic data across a Basin and Range normal fault, Crescent Valley, Nevada, *Tectonics*, *23*, TC2015, doi:10.1029/2003TC001528.
- Gourmelen, N., and F. Amelung (2005), Postseismic mantle relaxation in the central Nevada seismic belt, *Science*, *310*, 1473–1476.
- Hammond, W. C., and W. Thatcher (2005), Northwest Basin and Range tectonic deformation observed with the Global Positioning System, 1999–2003, *J. Geophys. Res.*, *110*, B10405, doi:10.1029/2005JB003678.
- Katzenstein, K. W., and J. Bell (2006), Bedrock Subsidence Associated with Mine-dewatering Identified by InSAR in Central Nevada, *Eos Trans. AGU*, *87*(52), Fall Meet. Suppl., H51D-0516.
- Lanari, R., O. Mora, M. Manunta, J. J. Mallorqui, P. Bernardino, and E. Sansosti (2004), A small-baseline approach for investigating deformation on full-resolution differential SAR interferograms, *IEEE Trans. Geosci. Remote Sens.*, *42*, 1377–1386.
- Malservisi, R., T. H. Dixon, P. C. La Femina, and K. P. Furlong (2003), Holocene slip rate of the Wasatch fault zone, Utah, from geodetic data: Earthquake cycle effects, *Geophys. Res. Lett.*, *30*(13), 1673, doi:10.1029/2003GL017408.
- Thatcher, W., G. R. Foulger, B. R. Julian, J. Svarc, E. Quilty, and G. W. Bawden (1999), Present day deformation across the Basin and Range Province, western United States, *Science*, *283*, 1714–1718.
- Watson, K. M., Y. Bock, and D. T. Sandwell (2002), Satellite interferometric observations of displacements associated with seasonal ground-water in the Los Angeles basin, *J. Geophys. Res.*, *107*(B4), 2074, doi:10.1029/2001JB000470.
- Wernicke, B., A. M. Friedrich, N. A. Niemi, R. A. Bennett, and J. L. Davis (2000), Dynamics of plate boundary fault systems from Basin and Range Geodetic Network (BARGEN) and geological data, *GSA Today*, *10*(11), 1–7.
- Wright, T. J., B. E. Parsons, and Z. Lu (2004), Toward mapping surface deformation in three dimensions using InSAR, *Geophys. Res. Lett.*, *31*, L01607, doi:10.1029/2003GL018827.

F. Amelung, F. Casu, M. Manzo, and R. Lanari, Istituto per il Rilevamento, Elettromagnetico dell'Ambiente, Consiglio Nazionale delle Ricerche, via diocleziano 328, I-80124 Napoli, Italy.

N. Gourmelen, Rosenstiel School of Marine and Atmospheric Science, Division of Marine Geology and Geophysics, University of Miami, 4600 Rickenbacker Causeway, Miami, FL 33149-1098, USA. (ngourmelen@rsmas.miami.edu)